Incorporating Daylight in buildings: a prediction approach using low-cost sky-luminance measurement device

Marshal S Maskarenj [a]****, Rangan Banerjee*** [b]***, Prakash C Ghosh*** [c]

[a,b,c] *Department of Energy Science and Engineering, Indian Institute of Technology Bombay, Powai, Mumbai, India*

Abstract: Building design optimization needs information of dynamic angular sky-luminance distribution, through measurement or models, for simulating indoor illuminance. Most simulation packages use standard sky-types of the established Commission International de l'Eclairage (CIE) sky-models for calculating sky-luminance data. However, owing to dynamic conditions of sky, there is a need for more realistic sky-data incorporating solar contribution, as compared to standard overcast skies. This paper presents a low-cost device for measuring angular sky-luminance distribution, and compares the measured datasets with established CIE standard skies. Proposed calibrated Light Dependent Resistor based device is used to measure the sky-luminance at various angles over time, and statistical analysis is performed on the measured datasets to determine the frequency of occurrence of various sky-types. Indoor predictions based on various datasets are calculated to assess accuracy of closest determined sky-type, and the applicability of the device for predicting indoor illuminance is demonstrated.

Keywords—Sky scanner, Sky luminance, Building daylighting, CIE sky models, Indoor daylight distribution, Daylight modeling

1. Introduction

Daylight has been integral to the evolution of human eyes, and has a positive physical and psychological effect on human mood, health and productivity (Aripin, 2007). A building design must incorporate adequate daylighting to be energy efficient while providing visual comfort to the occupants. Recommendations for an optimum design or for retrofits can be provided either through insight from metered physical systems, or through computational simulations: and since simulations cost much less than physical systems, it makes sense to focus on making validated simulation software. Multiple building simulation packages are available (Building Energy Software Tools, n.d.); however, there is a scope in improving the light simulation output. Evaluating the amount of electric light needed for providing the desired illuminance at a point in the room needs insights into the amount of available daylight: and a better daylight distribution prediction can enhance the accuracy of simulations. Sky component of daylight is angle-dependent and knowing the angular daylight distribution at discrete positions in the sky-dome can help calculate indoor daylight distribution through various avenues: windows, sky-lights and light guidance systems (Gago, Muneer, Knez, & Köster, 2015).

Assessing dynamic sky-luminance at discrete angles is challenging, and models have been used in place of measurement systems: advancing from the Lambertian overcast sky model (Kittler & Darula, 2016), to gradation based models (Moon & Spencer, 1942), to the presently accepted Commission International de l'Eclairage (CIE) sky models (Darula & Kittler, 2002). The present CIE model incorporates the gradation and scattering phenomena on daylight distribution, and through coefficients, proposes 15 most-probable sky-types. This model proposes 5 clear skies, 5 intermediate and 5 overcast skies (Li, Lau, & Lam, 2003); however, two of these sky-types are most preferred by simulation packages: the CIE standard overcast sky and the CIE standard clear sky model (Autodesk Help, 2017) — as industry standards. Almost all Daylight Factor calculations incorporate the overcast sky model, ignoring the effect of azimuth or sun-position. This affects the accuracy of indoor light calculations, since the indoor illuminance calculations are underestimated (Inanici & Hashemloo, 2017) as compared to their actual value due to difference in sky-luminance assessment. A sky-measurement system can highly enhance the accuracy of indoor illuminance predictions, either through dynamic data sharing on a centralized system at campus-levels, or through generating annual datasets. These standard annual datasets need to be created at various global locations, and need devices for measurement of angular luminance distribution of sky-hemisphere.

Literature provides designs for measuring luminance of pre-defined discrete sky-patches (Casares, Ramírez-Faz, & López-Luque, 2014; Kider, Knowlton, Newlin, Li, & Greenberg, 2014; Komar, Rusnak, & Dubnicka, 2013; Shahriar, 2010), and various works have employed a commercial system for sky-analysis (Li et al., 2003; Suárez-García, Granados-López, González-Peña, Díez-Mediavilla, & Alonso-Tristán, 2018; Wittkopf & Soon, 2007) at few locations. However, these devices are cost-intensive and/or lack the ruggedness for continuous operations due to use of fragile and cost-intensive parts like spectroradiometers. To counter challenges with projecting the sky-hemisphere on flat sensors, as proposed in few previous works, there is a need for device with sensors oriented towards specific sky-positions. This device needs to be low-cost for wider reach, and rugged for long term operations in exposed environments.

In our previous work, we have developed a low cost device for measurement of angular sky-luminance distribution — a Light Dependent Resistor-based system using Arduino microcontroller, and demonstrated its applicability in scanning the sky-dome (Maskarenj, Banerjee, & Ghosh, 2018) and identifying sky-types (Maskarenj, Chawla, Banerjee, & Ghosh, 2018a). We were able to develop the prototype for under $200, affordable for creating a wide network of scanning systems as compared to commercial device's landing cost of $35,000 (as of July 2017). The device used sensors placed on a semi-circular frame facing different altitudinal positions and the frame was rotated on a vertical axis to capture data through various azimuthal positions for each sensor.

In this work, we extend the previous approach and describe an improved prototype with more portability. This upgraded prototype uses a Fresnel-based arrangement of sensors, with less bulk and cheaper fabrication at about $80. Through this paper, the concept of the modified design is presented, a brief analysis of primary measured sky-data is discussed, and the applicability of the device in indoor illuminance predictions is proposed.

2. Sky luminance measurement system

Sensors on our previous device were mounted on a circular frame: this increased the cost of fabricating a rigid mount with fixed angles for mounting sensors, while also increasing the weight of the device. The upgrade uses a Fresnel-like placement of sensors — mounts oriented at various altitudinal placements were fixed linearly for sensor placement, as demonstrated in Figure 1. Sensors thus faced 12 different altitudinal positions: from Zenith till Zenith+82.5° in 7.5° intervals. The frame was rotated in 24 azimuthal positions with 15° interval to scan the hemisphere and capture the luminance of each patch

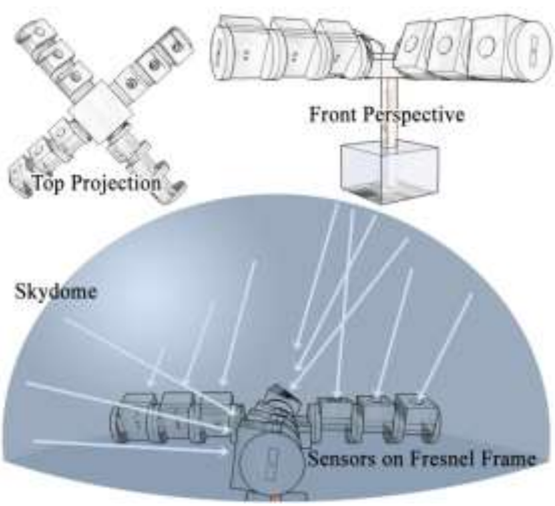

Fig. 1 - Fresnel-like design for sky-scanning device

3. Measurement of luminance at various sky-positions

Data was captured in 5-minute intervals from morning to evening, with datasets of 12x24 patch-luminance values. The brightest patch in each set was taken as the sun's position, as demonstrated in Figure 2. For most time-points, the sun-position was highly defined, but the dawn and dusk periods were more diffused, with non-singular and non-specific spots of peak brightness. For temporal analysis of measured data: comparing captured illuminance at different sky-patches, and for comparing measured illuminance with modeled datasets, 12 sky-positions with pre-defined alt-azimuth positions were chosen as demonstrated in Figure 3. The datasets were normalized: the average value of zenith was determined by averaging the calibrated luminance for 24-zenith data values, and each of the 288 patch-luminance values were factored with the zenith luminance. This generated normalized luminance datasets with values for 265 discrete patches (11x24 + Zenith). A python algorithm was scripted to interpolate these 12x24 normalized datasets to 90x360 datasets with 1° resolution. Thereafter, the cylindrical datasets were transposed to polar-coordinates to generate sky-maps like the commercial device. Each dataset with 5-minute interval for the test day (16 Nov 2017) was batch converted to polar-sky-map.

Fig. 2 - Solar trajectory through assessing brightest sky-positions

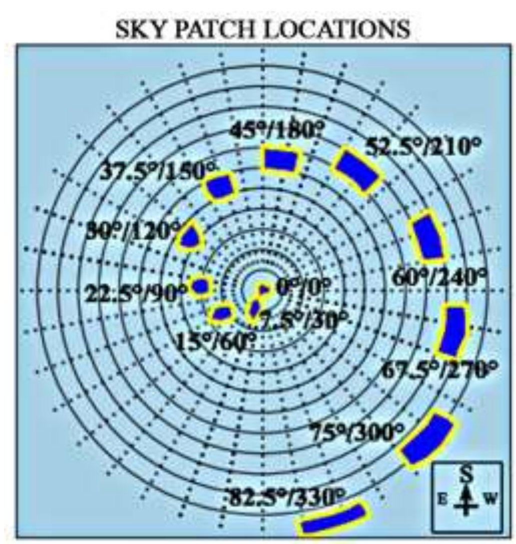

Fig. 3 - Sky positions used for analysis

Figure 4 demonstrates sky-maps of measured data for few time-points. A comparison of normalized patch luminance variation through the day for the 12 chosen patches (Figure 3) is presented in Figure 5.

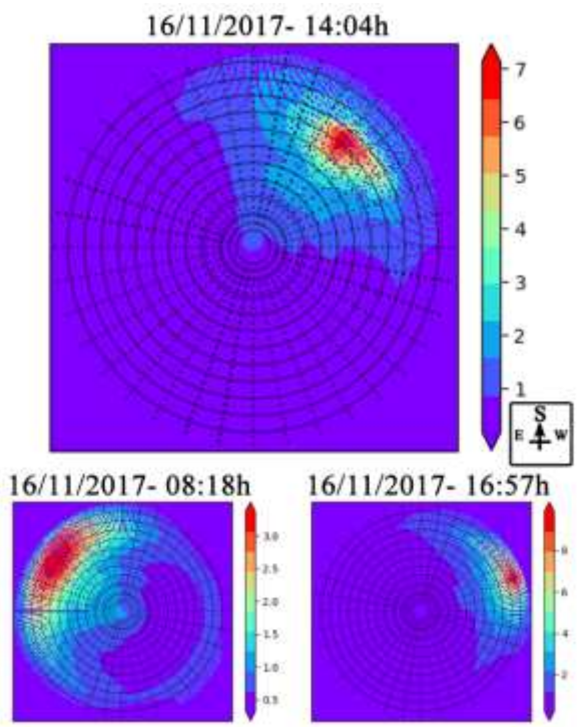

Fig. 4 - Measured normalized Sky-maps at few time points

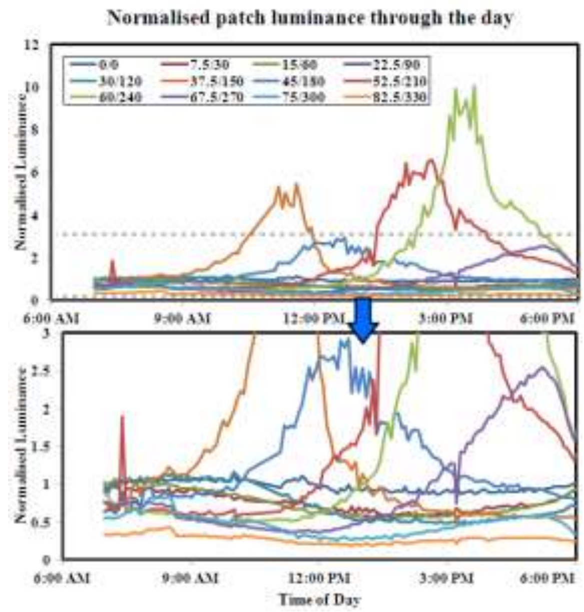

Fig. 5 - Luminance variation for 12 chosen sky-positions over the day

As seen in Figure 5, the luminance of patches in southern hemisphere: 37.5/150, 45/180, 52.5/210 and 60/240 shows peaks at different times of day, owing to proximity to sun-path (Figures 2 and 3). Zoomed-in lower section of Figure 5 shows the variation in luminance through the day for other patches.

4. Comparing Measurements with Models

The CIE model coupled with sun-position determined through measurements (Figure 2) was used to generate virtual sky-dome calculations for all 15 CIE skies. In the model, the luminance ratio of any sky-patch ($L\gamma\alpha$) with the zenith luminance (Lz) is defined as is Equation 1:

$$\frac{L_{\gamma\alpha}}{L_z} = \frac{f(\chi).\varphi(Z)}{f(Z_s).\varphi(0°)} \qquad (1)$$

Here, f() determines the scattering function while φ() determines the gradation function. The value of gradation function for any sky-patch at altitude Z and the gradation for zenith are calculated using Equations 2 and 3:

$$\varphi(Z) = 1 + a.\exp\left(\frac{b}{\cos(Z)}\right) \quad (2)$$

$$\varphi(0^\circ) = 1 + a.\exp(b) \quad (3)$$

The scattering function for any sky-patch at distance χ from the sun, and for zenith when the sun is at Zs distance are calculated as using Equations 4 and 5:

$$f(\chi) = 1 + c.\left(\exp(d.\chi) - \exp\left(d.\frac{\pi}{2}\right)\right) + e.\cos^2\chi \quad (4)$$

$$f(Z_s) = 1 + c.\left(\exp(d.Z_s) - \exp\left(d.\frac{\pi}{2}\right)\right) + e.\cos^2 Z_s \quad (5)$$

For a defined sun-position, the normalized distribution depends on the gradation coefficients (‘a’,‘b’) and the scattering coefficients (‘c’,‘d’,‘e’) presented in Table 1. Each virtual sky-dome represents either a clear, intermediate or overcast sky-type.

Table 1: Coefficients for various sky-types (Darula & Kittler, 2002)

	Sky	φ( )	f( )	a	b	c	d	e
Overcast	1	I	1	4.0	-0.7	0	-1.0	0.00
	2	I	2	4.0	-0.7	2	-1.5	0.15
	3	II	1	1.1	-0.8	0	-1.0	0.00
	4	II	2	1.1	-0.8	2	-1.5	0.15
	5	III	1	0.0	-1.0	0	-1.0	0.00
Inter-mediate	6	III	2	0.0	-1.0	2	-1.5	0.15
	7	III	3	0.0	-1.0	5	-2.5	0.30
	8	III	4	0.0	-1.0	10	-3.0	0.45
	9	IV	2	-1.0	-0.55	2	-1.5	0.15
	10	IV	3	-1.0	-0.55	5	-2.5	0.30
Clear	11	IV	4	-1.0	-0.55	10	-3.0	0.45
	12	V	4	-1.0	-0.32	10	-3.0	0.45
	13	V	5	-1.0	-0.32	16	-3.0	0.30
	14	VI	5	-1.0	-0.15	16	-3.0	0.30
	15	VI	6	-1.0	-0.15	24	-2.8	0.15

Figure 6 demonstrates a comparison between measured sky-map for a defined time-point with few modeled sky-types for the normalized values.

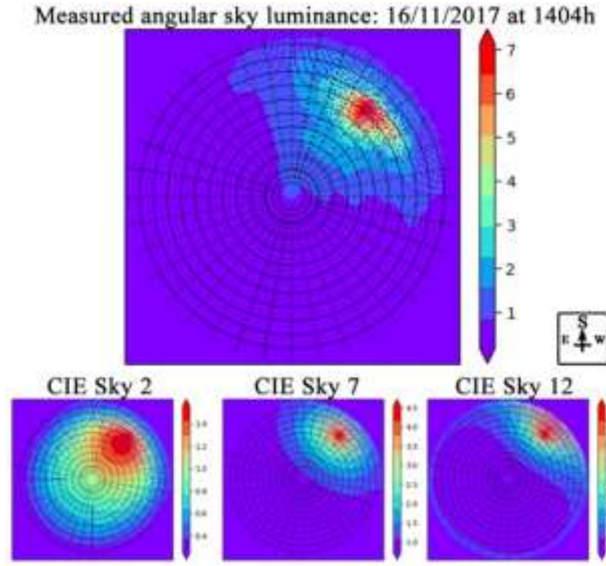

Fig. 6 – Comparing measured and modeled Sky-maps

For a quantitative analysis, the dynamic variation between a representative sky-position selected from primary analysis (Figure 5) — 37.5°/150° is analyzed. For various sky-models, the variation in patch luminance based on determined sun-position and model coefficients were calculated through the day and compared with the measured patch-luminance variation. Figure 7 shows the temporal patch-variation and the lower segment shows the closest sky-types for the measured normalized data.

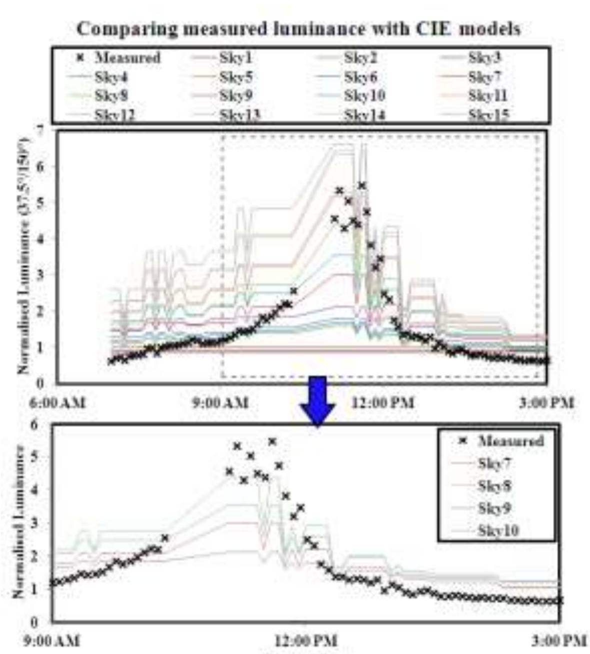

Fig. 7 – Comparing variations between measured and modeled luminance for 37.5/150 patch through the day (normalized data)

5. Identification of closest sky-type

Using RMSD approach (Li et al., 2003; Suárez-García et al., 2018), the normalized luminance values for each time-stamp were compared with the 15 modeled-datasets for the 265 sky-positions. The sky-type with minimum deviation with measured data was selected as the closest CIE sky-type for the time-point. For the entire day, the closest sky for 128 datasets was assessed to find the frequency of occurrence for different skies, as demonstrated in Figure 8.

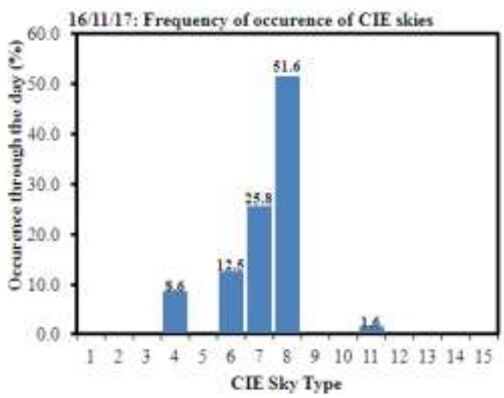

Fig. 8 – Frequency of occurrence using RMSD approach

CIE Sky-type 8 (Partly Cloudy sky, No gradation, distinct solar corona) is seen dominating more than 50% of the day (0700h-1815h). This approach may also be implemented to identify the closest sky through the day, and plot the change in sky-type through the day.

6. Application in indoor illuminance prediction

An algorithm is scripted in Python to calculate the indoor illuminance distribution based on angular sky-luminance datasets, given the dimensions of the room and the windows on defined facades. For simplicity, the angular transmissivity coefficient of window material is neglected (taken unity for all incident angles), assuming windows as cavity for daylight addition. The daylight-based illuminance at any point indoors is calculated based on the luminance of all sky-patches seen from the point in the interiors.

A room of 20 units by 20 units of height 8 units is taken for these calculations, with two windows at two adjacent walls facing the exterior (other two walls are assumed shared with other rooms), with the room geometry as shown in Figure 9.

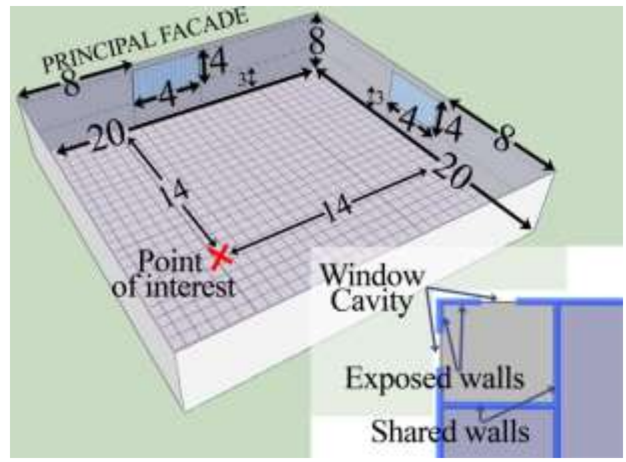

Fig. 9 – Schematics of room and windows used in calculations

The calculation based algorithm was fed sky-luminance datasets: modelled and measured. Standard skies of the CIE sky-model (sky type 1: CIE standard overcast sky, and sky type 12: CIE standard clear sky) along with the sky-type of highest frequency of occurrence (sky type 8: assessment based on protocol presented in section 5) were used to generate angular luminance datasets through various times of the day. Also, the measured angular sky-luminance dataset through the day was used for calculating indoor illuminance at the point of interest as shown in Figure 9. The point of interest was selected 14 units away from either exposed wall (a deeper point about 2/3 inside the room on either side) as demonstrated in Figure 9.

The calculations are done for three orientations of the principal facade: due east (90 degrees from north), south east (135 degrees from north) and due south (180 degrees from north orientation): with the secondary window facing due south, south-west and due west respectively.

Figure 10 demonstrates the indoor illuminance distribution at 1404h on 16 Nov 2017; the measured sky-luminance at this time-point is demonstrated in Figure 6. Sun position is around 45º SW, at an elevation of about 30 degree. With window facing at the sun-orientation, the illuminance calculated at 135 orientation based on measured sky-luminance dataset in Figure 10 demonstrates glare indoors. Orientation 180 has windows facing due south and due east, and cumulative illuminance pattern is seen. Orientation 90 has one window facing the sky-hemisphere opposite to sun-position, and the contribution from principal window facing due-east is minimal in indoor illuminance. The images are set for scale of 20,000 lux.

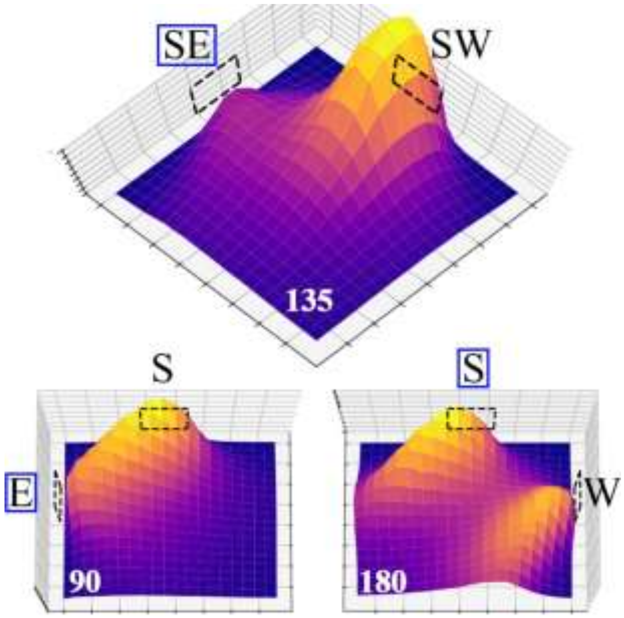

Fig. 10 – Illuminance distribution calculated at discrete points for three orientations of the principal façade based on measured sky-luminance dataset at 1404h on 16 Nov 2017 (Mumbai)

To compare the illuminance distribution arising from different modelled and measured datasets, the calculations done for the same time-point (1404h) is demonstrated in Figure 11 for four sky-luminance datasets: dataset generated using CIE standard overcast sky model (sky 1), dataset generated from CIE standard clear sky model (sky 12), dataset generated from CIE sky type 8 — the statistically closest sky-type, and the ambient sky-luminance dataset measured from the proposed device.

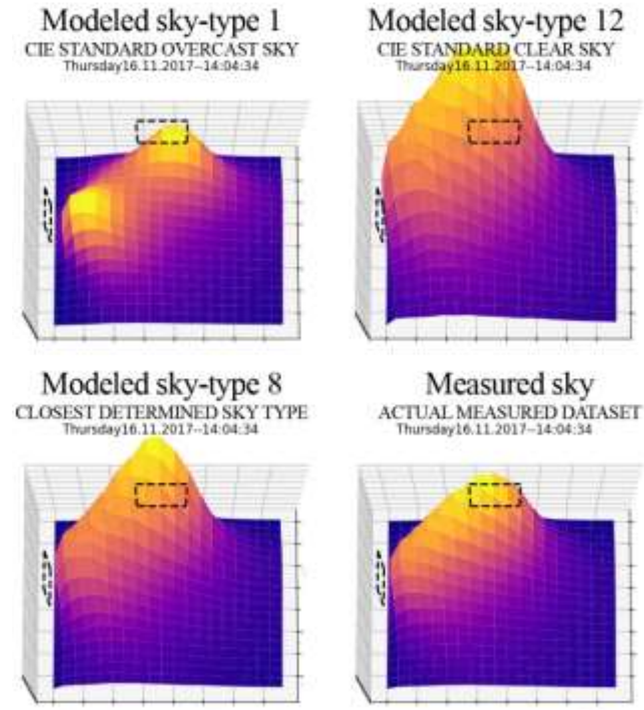

Fig. 11 – Comparison of indoor illuminance prediction at the same time-point (1404h) and same orientation (principal due east) for standard models, measured and assessed model datasets

As seen in Figure 11, the standard overcast sky (sky 1) highly underestimates the indoor illuminance predictions, while the standard clear sky model (sky 12) overestimates the indoor illuminance predictions. The prediction with sky-8 is seen in close limits with the calculations based on measured dataset.

To assess the proximity between the measurement-based prediction with various sky-models, the temporal variation at a specific point of interest is analysed. For the point of interest indicated in Figure 9 — a point placed deep in the room located 14 units from both walls with windows in the 20x20 room — the luminance variation was calculated through the day for the three orientations of the principal facade (90º, 135º and 180º), for the four datasets (sky 1, sky 8, sky 12 and measured). Figure 12(a) demonstrates the indoor illuminance variation through the entire day for four datasets for three orientations of the principal facade. Indoor prediction with principle facade facing orientation 135º for the four datasets is demonstrated in Figure 12 (b). As seen for 135º orientation, the point of interest faces a dark-zone between the windows between ~1000h and ~1400h, and has a much lower illuminance range in this period as compared to the illuminance through the day.

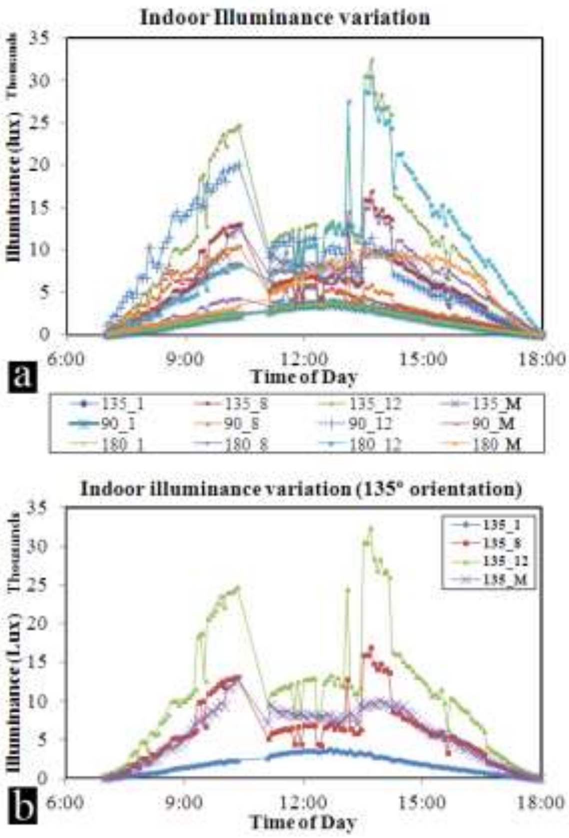

Fig. 12 – Variation in calculated indoor illuminance at the point of interest through measured and modeled datasets: (a) At various orientations of principal façade, and (b) Principal façade facing 135°.

As demonstrated in Figure 12(b), the CIE standard overcast sky (sky 1) predicts much lower illuminance, while standard clear sky (sky 12) predicts much higher illuminance at the point of interest. Using RMSD technique for the numbers presented in Figure 12(b), the RMSD between measured dataset and datasets generated for sky-types 1, 8 and 12 is 4546 lux, 2014 lux and 7422 lux, respectively through the day. Sky type 8 thus demonstrates minimum deviation in indoor prediction as compared to predictions from the measured dataset, as compared with generic sky-model based calculations.

7. Discussion

This work is significant, since there is a considerable margin between the cost of our previously discussed device (Maskarenj, Banerjee, et al., 2018) and the commercial device, and we have further reduced the cost and the bulk using a modified frame for sensor mounting. The device is more portable and lightweight. A low cost device can be used as a centralized sensor for buildings in a campus area for mapping the dynamic sky-component at various angles, since the angular sky-luminance distribution over this area may be assumed same at any given time. This information may be fed into building management devices that can compute the luminance distribution in various facilities using virtual sensor-positions, and control the electric lights through dimming and switching off. Shading devices may also be automated. This eliminates the need for multiple actual sensors places through individual rooms over the campus, and a singular device may be used along with an algorithm for predicting indoor daylight distribution using measured sky-component of daylight at discrete angles. Another significant use of this device is towards generating datasets, which may be used as input along with weather data in simulation software; thus using a more realistic sky-dome as compared to overcast model-based virtual sky-dome. This approach can help optimize building designs towards better daylight addition, using high accuracy simulations in their pre-construction phase.

8. Conclusions

An upgraded design for a low-cost LDR-based sky-luminance measurement system is discussed. The device is used to measure sky-luminance at 265 sky-positions and the measured data for few specified locations and time-points is analyzed. CIE models are used to generate modeled datasets for all 15 CIE-skies for each time-point. Statistical analysis is done between measured and modeled datasets, and frequency of occurrence for various closest CIE skies is determined for test day. Indoor illuminance predictions through modeled sky-luminance datasets and with closest recommended sky-models are compared with the illuminance predictions based on actual measured sky-luminance datasets for validity of recommended sky-type. An extension of this approach may identify closest CIE sky types through the day, recommending the closest sky-type for various time-points in a dataset.

9. Acknowledgements

The first author would like to acknowledge Mr. Gaurav Chawla for helping in device development, and Dr. Ronita Bardhan for the insightful discussions

10. Additional Information

The details of design and development of the original prototype are filed under Indian Patent Application 201821007607 (pending) filed on 28 Feb 2018(Maskarenj, Chawla, Banerjee, & Ghosh, 2018b).

References

Aripin, S. (2007). 'Healing Architecture': Daylight in Hospital Design. *Sustainable Building South East Asia*, (November), 5–7.

Autodesk Help. (2017). CIE Sky Model | 3ds Max | Autodesk Knowledge Network. Retrieved April 29, 2018 (online).

Building Energy Software Tools. (n.d.). Software Listing | Best Directory. Retrieved October 6, 2016 (online).

Casares, F. J., Ramírez-Faz, J., & López-Luque, R. (2014). Development of synthetic hemispheric projections suitable for assessing the sky view factor on horizontal planes. *Energy and Buildings*, *82*, 696–702. http://doi.org/10.1016/j.renene.2014.08.025

Darula, S., & Kittler, R. (2002). CIE General sky standard defining luminance distributions. *ESim*, 8.

Gago, E. J., Muneer, T., Knez, M., & Köster, H. (2015). Natural light controls and guides in buildings. Energy saving for electrical lighting, reduction of cooling load. *Renewable and Sustainable Energy Reviews*, *41*, 1–13.

Inanici, M., & Hashemloo, A. (2017). An investigation of the daylighting simulation techniques and sky modeling practices for occupant centric evaluations. *Building and Environment*, *113*, 220–231.

Kider, J. T., Knowlton, D., Newlin, J., Li, Y. K., & Greenberg, D. P. (2014). A framework for the experimental comparison of solar and skydome illumination. *ACM Transactions on Graphics*, *33*(6), 1–12. http://doi.org/10.1145/2661229.2661259

Kittler, R., & Darula, S. (2016). Scattered sunlight determining sky luminance patterns. *Renewable and Sustainable Energy Reviews*, *62*, 575–584. http://doi.org/10.1016/j.rser.2016.05.012

Komar, L., Rusnak, A., & Dubnicka, R. (2013). Analysis of diffuse irradiance from two parts of sky vault divided by solar meridian using portable spectral sky-scanner. *Solar Energy*, *96*, 1–9. http://doi.org/10.1016/j.solener.2013.07.003

Li, D. H. W., Lau, C. C. S., & Lam, J. C. (2003). A Study of 15 Sky Luminance Patterns against Hong Kong Data. *Architectural Science Review*, *46*(February 2014), 61–68.

Maskarenj, M., Banerjee, R., & Ghosh, P. C. (2018). Design and development of a low-cost angular sky luminance measurement system. *Building and Environment*. http://doi.org/10.1016/j.buildenv.2018.06.001

Maskarenj, M., Chawla, G., Banerjee, R., & Ghosh, P. C. (2018a). Evaluation of dynamic sky-type using novel angular sky luminance measurement system. *Building and Environment*. http://doi.org/10.1016/j.buildenv.2018.09.051

Maskarenj, M., Chawla, G., Banerjee, R., & Ghosh, P. C. (2018b). Light Dependent Resistor based angular Daylight distribution measurement device. India.

Moon, P., & Spencer, D. (1942). Illumination from a non-uniform sky. *Trans Illum Eng Soc*, *37*, 707–726.

Shahriar, A. N. M. (2010). Exploration into sky brightness capture through digital camera configuration. In *44th annual conference of the Architectural Science Association, ANZAScA 2010*.

Suárez-García, A., Granados-López, D., González-Peña, D., Díez-Mediavilla, M., & Alonso-Tristán, C. (2018). Seasonal caracterization of CIE standard sky types above Burgos, northwestern Spain. *Solar Energy*, *169*(January), 24–33.

Wittkopf, S. K., & Soon, L. K. (2007). Analysing sky luminance scans and predicting frequent sky patterns in Singapore. *Lighting Research and Technology*, *39*(1), 31–51.